Letter

Helium-nitrogen mixtures at high pressure

Jingyu Hou,[1,2] Xiao-Ji Weng,[1,2] Artem R. Oganov,[3] Xi Shao,[2] Guoying Gao,[2] Xiao Dong,[1,*] Hui-Tian Wang,[1] Yongjun Tian,[2] and Xiang-Feng Zhou[1,2,†]

[1]*Key Laboratory of Weak-Light Nonlinear Photonics and School of Physics, Nankai University, Tianjin 300071, China*

[2]*Center for High Pressure Science, State Key Laboratory of Metastable Materials Science and Technology, School of Science, Yanshan University, Qinhuangdao 066004, China*

[3]*Skolkovo Institute of Science and Technology, Skolkovo Innovation Center, 3 Nobel Street, Moscow 143026, Russia*

(Received 4 March 2020; revised 29 December 2020; accepted 19 January 2021; published 4 February 2021)

The energy landscape of helium-nitrogen mixtures is explored by *ab initio* evolutionary searches, which predicted several stable helium-nitrogen compounds in the pressure range from 25 to 100 GPa. Among these high-pressure compounds, the monoclinic structure of HeN_{22} consists of neutral He atoms, partially ionic dimers $N_2^{\delta-}$, and lanternlike cages $N_{20}^{\delta+}$, showing a certain amount of charge transfer within the nitrogen framework. The monoclinic $(HeN_{20})^{\delta+}N_2^{\delta-}$ may be quenchable to ambient pressure with the estimated energy density of 10.44 kJ/g, which is ∼2.4 times larger than that of trinitrotoluene, indicating a very promising high-energy-density material.

DOI: 10.1103/PhysRevB.103.L060102

Helium is the most inert and second most abundant element in the universe. Helium has the highest ionization potential among all elements (25 eV) and zero electron affinity, both of which are related to its closed-shell electronic structure, it generally does not interact with other elements or compounds under ambient conditions [1]. However, the chemistry of the elements can be greatly altered by pressure [2–6]. Even an element as inert as helium can display some reactivity at high pressure. For example, the already synthesized Na_2He and the predicted Na_2HeO, $FeHe_x$, and other helium-bearing compounds possess unusual properties, some of them being electrides and some being superionic conductors, and such compounds may retain helium in the interiors of earth and other planets [6–12]. Hence, high-pressure helium-bearing compounds are of great interest to fundamental physics, chemistry, and earth and space sciences. At the same time, helium reacts with elements and compounds and forms solid van der Waals (vdW) compounds such as $He(N_2)_{11}$ [13], $NeHe_2$ [14], and $He@H_2O$ [12,15]. For these materials, the enthalpy of formation is close to zero, and the removal of helium has little effect on the host's properties. At high pressure, helium occupies empty spaces in the structure, helping to improve its packing efficiency. This may stabilize those crystal structures that have cavities of suitable size to host helium and can be used to synthesize new metastable structures when helium atoms are removed.

At ambient conditions, pure nitrogen exists in the form of a gas of diatomic molecules. The chemistry of nitrogen is dramatically altered under high pressure because the particularly strong triple N ≡ N bond transforms into a much weaker single N-N bond. The average bond energy of N ≡ N (945 kJ/mol) is almost 6 times larger than that of single N-N (160 kJ/mol); thus, huge energy is realeased when single N-N bonds revert to triple N ≡ N bond at ambient pressure. Consequently, singly bonded nitrogen-rich compounds are excellent candidates for high-energy-density materials. The search for polymeric nitrogen or nitrogen-rich materials has attracted enormous attention due to the potential applications for energy storage, explosives, and propellants [16–31]. Direct synthesis of single-bonded polymeric nitrogen is extremely challenging because of high activation barriers for their formation. For instance, the successfully synthesized polymeric nitrogen allotrope in the so-called cubic gauche structure (denoted as cg-N) was synthesized in 2004 [19], long after its prediction and (because of high barriers and metastable persistence of lower-pressure phases) at pressures two times higher than predicted, and is metastable at least down to 25 GPa [19,20]. After that, layered polymeric nitrogen with *Pba*2 symmetry (denoted as LP-N), layered polymeric nitrogen with $P4_2bc$ symmetry (denoted as HLP-N), and nitrogen with black phosphorus structure (denoted as bp-N) were synthesized in succession [26,29–31]. Overall, the calculated high-pressure zero-temperature phase diagram of polymeric nitrogen was extensively studied with the established sequence of cg-N → LP-N (188 GPa) → N_{10} (263 GPa) → *Cmca* metal (2.1 TPa) → $P4/nbm$ metallic salt (2.5 TPa) [29]. The challenge is to synthesize single-bonded nitrogen structures at moderate pressures, and to preserve them at ambient conditions. Therefore, helium-nitrogen mixtures may provide an alternative way to achieve this goal at high pressure [7,13,32,33]. The solid vdW compound $He(N_2)_{11}$ was successfully synthesized at room temperature and 9 GPa, and persisted up to 135 GPa [13,32,33], but we are interested primarily in the likely high-pressure polymeric compounds.

*xiao.dong@nankai.edu.cn

†xfzhou@nankai.edu.cn; zxf888@163.com

Here, the variable-composition evolutionary algorithm USPEX was utilized to predict all stable He-N compounds [34,35]. At each pressure, both the structure and the He:N concentrations were varied simultaneously. In this way, there was an unbiased sampling of the entire range of concentrations. Our searches had up to 40 atoms per primitive cell and were performed at pressures of 25, 50, 75, and 100 GPa [36]. A compound is deemed stable at zero temperature if its enthalpy of formation ΔH from the elements and from any isochemical mixture of other compounds is negative [2,3,6,37,38]. Here the enthalpy of formation is defined as $\Delta H = H(\mathrm{He}_{1-x}\mathrm{N}_x) - (1-x)H(\mathrm{He}) - xH(\mathrm{N})$. For all stable compounds (i.e. those located on the convex hull), fixed-composition evolutionary searches were carried out to ensure the lowest-enthalpy structures. Note that the calculated transition pressure from molecular ϵ-N_2 to solid cg-N is about 56 GPa [Fig. S1(a) in the Supplemental Material] [36]. However, due to the large activation barrier, ϵ-N_2 experimentally transformed into cg-N at pressures above 110 GPa and temperatures above 2000 K [19], and thus, the ϵ-N_2 molecular structure is used for pure nitrogen [7]. Structure relaxations and calculations of the electronic properties were conducted in the framework of density functional theory (DFT) within the generalized gradient approximation GGA using the Perdew-Burke-Ernzerhof (PBE) functional [39], as implemented in the VASP code [40]. We employed the all-electron projector augmented wave [41] potentials with valence shells $1s^2$ and $2s^2 2p^3$ for He and N, respectively. A plane-wave cutoff energy of 500 eV and uniform Γ-centered k meshes with a resolution of $2\pi \times 0.06$ Å^{-1} were adopted for USPEX searches. They were further increased to 700 eV and $2\pi \times 0.03$ Å^{-1} for precise energy and property calculations. To examine the importance of vdW interactions on thermodynamic stability, the semiempirical dispersion-correction method was used but produced practically identical results [42]. Phonon dispersion curves were calculated with the PHONOPY code using the finite-displacement method [43]. In addition, the crystal orbital Hamiltonian population (COHP) method [44] implemented in the LOBSTER package was utilized for chemical bonding analysis (including the Mulliken and Löwdin population analysis) [45].

The convex hulls in Fig. 1 show several stable helium-nitrogen compounds at different pressures. First, the vdW compound HeN_4 with $P4/ncc$ symmetry is stable in the pressure range from 0 to 68 GPa (denoted as $P4/ncc$ HeN_4; a similar designation was applied for other He-N compounds). Second, other unprecedented polymeric forms, namely, $P6_3/m$ HeN_{10}, $C2/m$ HeN_{22}, and $R\bar{3}m$ HeN_6, are stabilized above 64 GPa. The pressure-composition phase diagram of the He-N system is shown in Fig. S1(b) [36]. The corresponding stabilization pressures for $P6_3/m$ HeN_{10}, $C2/m$ HeN_{22}, and $R\bar{3}m$ HeN_6 are 64.3, 67.6, and 74 GPa, respectively. The only synthesized He-N compound has the stoichiometry $He(N_2)_{11}$, and its structure was determined by single-crystal x-ray diffraction [$P6_3/m$ $He(N_2)_{11}$] [33]. However, we are unable to study such a structure within the present *ab initio* calculations because of the orientational disorder of the N_2 molecules in it and fractional atomic occupancies. Nevertheless, the successful synthesis of $P6_3/m$ $He(N_2)_{11}$ may imply the existence of polymeric HeN_{22} or other He-N compounds at extreme conditions. The variable-cell nudged elastic band method [46,47] was used to evaluate the energy barriers and paths for the formation of $C2/m$ HeN_{22} at various pressures. The calculated energy barriers are 1.08, 0.34, and 0.14 eV/atom at 0, 50, and 100 GPa (Fig. S2), indicating that the reaction barrier decreases with pressure [36]. Therefore, the proposed structures may be obtained in diamond anvil cell experiments at high pressures and temperatures.

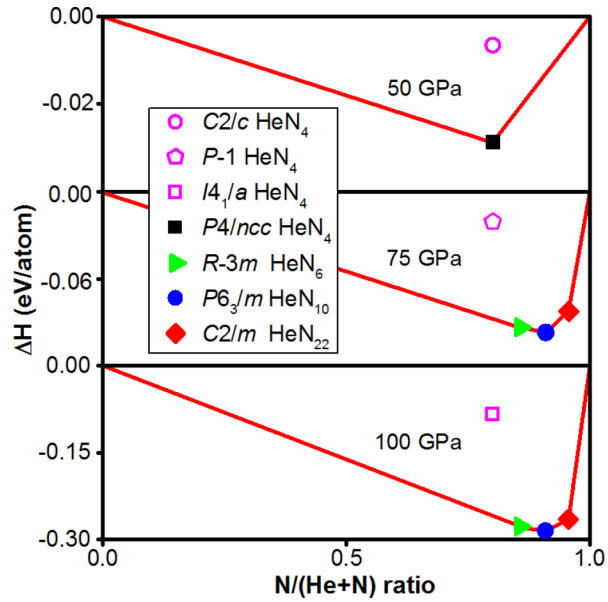

FIG. 1. Predicted convex hulls of the He-N system at selected pressures, using hcp-He and ϵ-N_2 structures for reference. The reported structures of HeN_4 [7] with symmetries $C2/c$, $P\bar{1}$, and $I4_1/a$ are plotted for comparison.

Lattice parameters and atomic positions of various structures are listed in Table SI [36]. As shown in Fig. 2(a), $P4/ncc$ HeN_4 is a tetragonal vdW compound with eight N_2 molecules per unit cell in different orientations. The length of triple N ≡ N bonds in $P4/ncc$ HeN_4 is ∼1.1 Å at 50 GPa, the same as in ϵ-N_2 and $C2/c$ HeN_4 [7]. The different packing of N_2 molecules in $P4/ncc$ HeN_4 results in greater density, smaller volume, and lower enthalpy than $C2/c$ HeN_4 at all pressures, explaining why the previously predicted $C2/c$ HeN_4 is not stable [7]. The band structure from the GGA-PBE calculation shows that $P4/ncc$ HeN_4 is an insulator with a band gap of 4.92 eV at 50 GPa [Fig. S3(a)] [36]. As pressure increases above 64.3 GPa, the triple N ≡ N bonds break and transform into single N-N bonds. The polymeric structure of $P6_3/m$ HeN_{10} emerges and is followed by $C2/m$ HeN_{22} and $R\bar{3}m$ HeN_6. They may coexist at 75 GPa and above. As shown in Fig. 2(b), $P6_3/m$ HeN_{10} has three inequivalent nitrogen atoms with Wyckoff positions $2d$, $6h$, and $12i$, with the former having sp^2 hybridization, while the other sites are sp^3. sp^2 N has planar triangular coordination, whereas sp^3 N has pyramidal "umbrella" coordination. There is a distinct difference in the distribution of lone pairs between sp^2 N and sp^3 N. The electron localization function shows that its maxima related to lone pairs point symmetrically on either side of sp^2 N, while pointing only in one direction on top of sp^3 N (Fig. S4) [36]. The band structure shows that

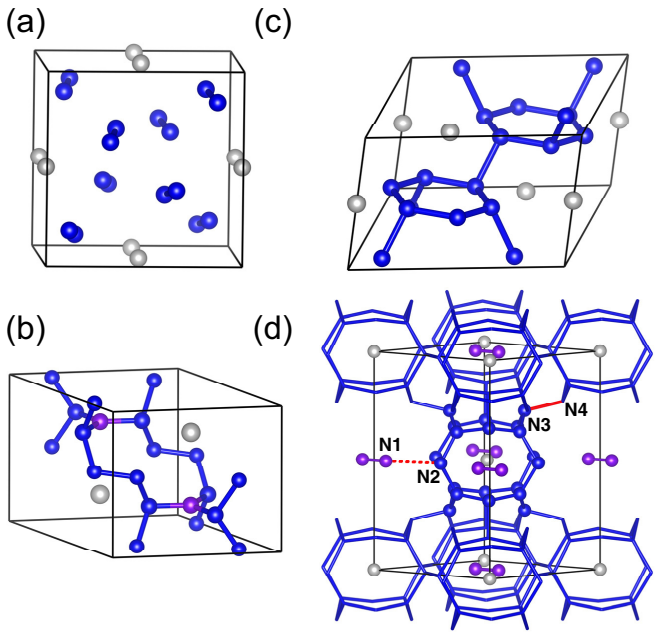

FIG. 2. Crystal structures of (a) $P4/ncc$ HeN_4 at 50 GPa, (b) $P6_3/m$ HeN_{10} at 100 GPa, (c) $R\bar{3}m$ HeN_6 at 100 GPa, and (d) $C2/m$ HeN_{22} at 100 GPa. To show structure features of $C2/m$ HeN_{22} more clearly, a nonstandard coordinate system is used. [36] The He atoms and N_2 dimers in HeN_{22} and sp^2 N in HeN_{10} are colored in gray and purple, respectively. The nearest distance between N_2 dimers and N_{20} cages is N1-N2 (red dotted line), while the shortest intercage N_{20} bond is N3-N4.

$P6_3/m$ HeN_{10} is an insulator with a band gap of 4.05 eV at 100 GPa [Fig. S3(b)] [36].

$R\bar{3}m$ HeN_6 is stable in the pressure range from 74 GPa to at least 110 GPa, and its structure consists of He and sp^3 N simultaneously. The nitrogen framework is made of distorted N_6 hexagons [Fig. 2(c)]. Each N atom has threefold coordination: two bonds are used to form the N_6 hexagon and have length of 1.31 Å at 100 GPa, while the other connects N_6 hexagons and has a length of 1.41 Å, which corresponds to a slightly compressed single N-N bond. Since the intrahexagonal N-N bonds are stronger (shorter) than those interhexagonal bonds, such peculiar bonding configurations indicate that neutral aromatic hexazine N_6 may be observed on decompression if the weak interhexagonal N-N bonds break first. The band structure shows that $R\bar{3}m$ HeN_6 is an insulator with a band gap of 3.42 eV at 100 GPa [Fig. S3(c)] [36].

Since the stoichiometry of $He(N_2)_{11}$ is known experimentally, the polymeric compound HeN_{22} may attract more interest among four newly predicted phases. As shown in Fig. 2(d), $C2/m$ HeN_{22} contains He atoms encapsulated in cages, interstitial N_2 dimers, and polymeric lanternlike N_{20} cages. The bond length in the N_2 dimer is 1.09 Å, the strongest bonds in this compound. The exotic lanternlike N_{20} cage contains 20 N atoms, with the faces of this cage being irregular N_8 rings [Fig. 2(d)]. The intracage bond lengths range from 1.28 to 1.34 Å at 100 GPa, while the intercage bond lengths range from 1.38 to 1.42 Å, indicating that intercage N-N bonds are weaker than intracage bonds. One helium atom is enclosed in the center of each N_{20} cage (the nearest He-N is ∼1.96 Å). The nearest distance between the N_2 dimer and N_{20} cage is ∼2.2 Å; no covalent bond exists between these two units, but there is an electrostatic interaction.

Based on the above-mentioned unique structures, Bader analysis of the total electron density was performed to investigate the charge transfer [48]. Charge transfer between He and N in $P4/ncc$ HeN_4, $R\bar{3}m$ HeN_6, $P6_3/m$ HeN_{10}, and $C2/m$ HeN_{22} is less than 0.05 $|e|$, and remains almost unchanged at various pressures, implying no real charge transfer between He and N. Unexpectedly, there is a much larger amount of charge transfer between N_2 dimers and N_{20} cages at 100 GPa. As summarized in Table SII [36], the N_2 dimers are negatively charged (−0.19 $|e|$) and serve as anions, while the positively charged N_{20} cages (+0.24 $|e|$) act as cations. Since helium is enclosed in the center of the N_{20} cage, the structure of $C2/m$ HeN_{22} could be viewed as $(HeN_{20})^{\delta+}N_2^{\delta-}$ ($\delta \approx 0.19$ $|e|$ at 100 GPa). The value of δ increases on increasing pressures ($\delta \approx 0.22$ $|e|$ at 150 GPa), while it is about 0.1 $|e|$ at zero pressure. For comparison, the calculated Mulliken and Löwdin [45] charges in $C2/m$ $(HeN_{20})^{\delta+}N_2^{\delta-}$ at 100 GPa are ∼0.22 $|e|$ and 0.25 $|e|$, respectively. All results from different methods are consistent with each other. Previously, the all-nitrogen "metallic salt" $N_2^{\delta+}N_5^{\delta-}$ ($\delta = 0.37$ $|e|$) was predicted to be stable above 2.5 TPa [25]. We therefore suggest that the framework of $N_{20}^{\delta+}N_2^{\delta-}$ resembles a partially ionic nitrogen clathrate structure at high pressure. Emergence of charge transfer was also observed in γ boron [49], yet this is a different case from nitrogen. Boron is electron deficient and forms icosahedron-based structures. The multicenter bonding and the charge transfer on some B-B bonds play a decisive role in structural diversity and stability. In contrast, nitrogen is an electron-rich element. The packing efficiency of lone pair electrons is crucial for the formation of various high-pressure phases rather than charge transfer [19,24].

The additional evidence for charge transfer in $C2/m$ $(HeN_{20})^{\delta+}N_2^{\delta-}$ is revealed by the charge density difference distribution, defined as $\Delta\rho = \rho(HeN_{22}) - \rho(He) - \rho(N_2) - \rho(N_{20})$, where $\rho(HeN_{22})$, $\rho(He)$, $\rho(N_2)$, and $\rho(N_{20})$ are the total charge densities of the whole structure and the sublattices of He, N_2 dimers, and polymeric N_{20} cages. Charge transfer can be examined from the region of negative $\Delta\rho$ to that of positive $\Delta\rho$ [50]. As shown in Figs. 3(a) and 3(b), the N_2 dimers are surrounded with big bubblelike charge accumulations, showing a significant positive differential charge (colored in yellow), while the small ellipsoid-shaped differential charge is attached to the vertices of N_{20} cages [Fig. 3(a)]. Analyzing regions of charge accumulation and depletion, we see that overall charge is transferred from N_{20} cages (lone pairs dominantly) to N_2 dimers. This result is consistent with Bader analysis.

The orbital-resolved band structure shows that $C2/m$ $(HeN_{20})^{\delta+}N_2^{\delta-}$ is an insulator with a DFT band gap of 3.67 eV at 100 GPa [Fig. 3(c)]. The highest valence band is due to hybridization of $2p$ states between N_2 dimers and N_{20} cages [Fig. 3(d)], implying the existence of fundamental interaction. To determine such an interaction, the COHP curves were calculated for bonding character analysis. A negative COHP indicates bonding, while a positive one indicates antibonding [51]. The calculated projected COHP curves

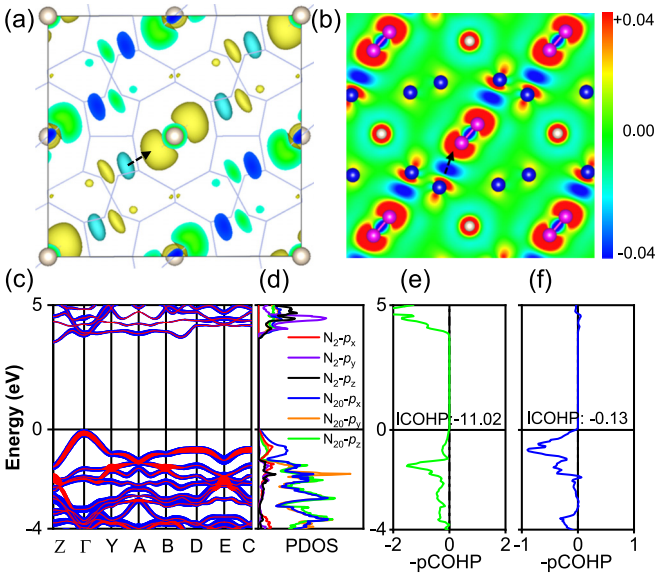

FIG. 3. Electronic properties of $C2/m$ HeN_{22} at 100 GPa. (a) and (b) As the dotted black arrow indicates, the charge density difference distribution shows that a notable charge transfer from N_{20} cages to N_2 dimers. (c) and (d) Band structure and projected density of states (PDOS). The orientation of N_2 dimers is set as the x axis. (e) and (f) The projected crystal orbital Hamiltonian population (pCOHP) for the shortest intercage N3-N4 bonds is in (e), and those (N1-N2) between N_2 dimers and N_{20} cages are in (f).

(-pCOHP < 0) for the shortest N-N of N_{20} cages or between N_2 dimers and N_{20} cages are both negative in the vicinity of the Fermi level E_F, clearly indicative of antibonding states [Figs. 3(e) and 3(f)]. The integrated COHP (ICOHP) up to E_F is -11.02 eV/pair for the shortest intercage N3-N4 [Figs. 3(e) and 2(d)], while it is -0.13 eV/pair for the nearest N1-N2 between N_2 dimers and N_{20} cages [Figs. 3(f) and 2(d)]. This clearly suggests that the intercage N-N bonds are strong and covalent, whereas the results are consistent with a weak interaction with some degree of ionicity (charge transfer) between the N_2 dimer and N_{20} cage. Therefore, the partially ionic nitrogen clathrate structure of $N_{20}^{\delta+}N_2^{\delta-}$ is confirmed again.

For all predicted helium-bearing nitrogen-rich compounds, it is natural to consider whether or not these high-pressure phases can be quenchable to ambient pressure and to examine the kinetic stability of the nitrogen framework after the removal of helium atoms. Therefore, we calculated phonon dispersion curves for these structures at relevant pressure ranges. The results show that $P4/ncc$ HeN_4 is dynamically stable at 50 GPa as there are no imaginary phonon frequencies in the whole Brillouin zone, and so are $R\bar{3}m$ HeN_6, $P6_3/m$ HeN_{10}, and $C2/m$ $(HeN_{20})^{\delta+}N_2^{\delta-}$ at 100 GPa (Fig. S5) [36]. Interestingly, phonon dispersion curves show that polymeric HeN_{10} and $(HeN_{20})^{\delta+}N_2^{\delta-}$ are dynamically stable at zero pressure (Fig. S6) [36], whereas the $P4/ncc$ HeN_4 and $R\bar{3}m$ HeN_6 phases are not (thus, zero-pressure properties of these unstable phases will not be discussed further). Moreover, the relaxed pure nitrogen structures, $P6_3/m$ N_{10} and $C2/m$ $N_{20}^{\delta+}N_2^{\delta-}$, are both dynamically stable at ambient

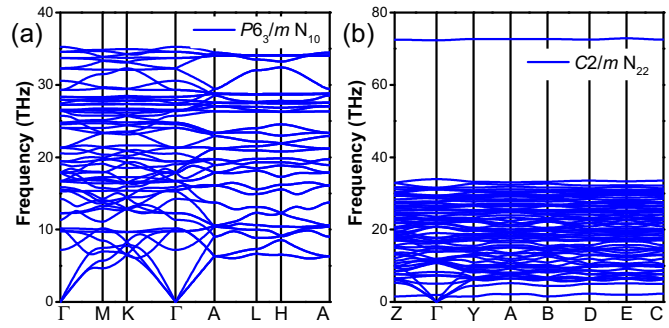

FIG. 4. Phonon dispersion curves of (a) $P6_3/m$ N_{10} and (b) $C2/m$ N_{22} at zero pressure.

pressure (Fig. 4). To further examine the thermal stability of $C2/m$ $(HeN_{20})^{\delta+}N_2^{\delta-}$, *ab initio* molecular dynamics simulations show that the $(HeN_{20})^{\delta+}N_2^{\delta-}$ structure is thermally stable up to 1000 K at ambient pressure (Fig. S7) [36]. The existence of thermodynamic stability implies that $C2/m$ $(HeN_{20})^{\delta+}N_2^{\delta-}$ or $P6_3/m$ HeN_{10} may be quenchable to ambient pressure.

The polymeric nitrogen-rich structures of $P6_3/m$ HeN_{10} and $C2/m$ $(HeN_{20})^{\delta+}N_2^{\delta-}$ are natural candidates for high-energy-density materials regardless of the presence of helium. The energy difference between a material and its decomposition products is utilized to evaluate the energy density [7,36,52–57]. On the basis of such a definition, the ground-state structures of N_{10} and $N_{20}^{\delta+}N_2^{\delta-}$ possess the same energy density of 10.44 kJ/g (Table SIII), showing that helium and partially charged $N_2^{\delta-}$ dimers do not make a contribution to the energy density owing to the weak interaction with the neighboring $N_{20}^{\delta+}$ cages. The estimated energy density of $C2/m$ $N_{20}^{\delta+}N_2^{\delta-}$ or $P6_3/m$ N_{10} is ~2.4 times larger than that of trinitrotoluene (TNT; 4.3 kJ/g) and 1.8 times larger than that of 1,3,5,7-tetranitro-1,3,5,7-tetrazoctane (HMX; 5.7 kJ/g) [53]. In addition, we estimated the detonation velocity D and pressure P, as other important factors for the performance of high-energy-density materials, using empirical Kamlet-Jacobs formulae [54] with $D = 1.01(NM^{0.5}Q^{0.5})^{0.5}(1 + 1.30\rho)$ and $P = 15.58\rho^2 NM^{0.5}Q^{0.5}$, where ρ, Q, N, and M represent the density, energy density, moles of dinitrogen gas per gram of explosives (mol/g), and the molar mass (g/mol) for dinitrogen gas [52,55], respectively. As shown in Table SIII [36], the detonation velocity and pressure for $P6_3/m$ N_{10} (21.59 km/s and 2660 kbar) and $C2/m$ $N_{20}^{\delta+}N_2^{\delta-}$ (22.67 km/s and 3006 kbar) are much higher than those of TNT (6.9 km/s and 190 kbar) and HMX (9.1 km/s and 393 kbar). All these values indicate that $P6_3/m$ N_{10} and $C2/m$ $N_{20}^{\delta+}N_2^{\delta-}$ are very promising high-energy-density materials.

In summary, we performed extensive structure searches for the high-pressure phases of helium-nitrogen mixtures and identified four stable compounds of HeN_4, HeN_6, HeN_{10}, and HeN_{22} at relevant pressure ranges. Among these predicted structures, a polymeric phase of HeN_{22} consists of neutral He, partially charged $N_2^{\delta-}$ dimers, and $N_{20}^{\delta+}$ cages. In particular, the unique partially ionic nitrogen clathrate structure $(N_{20}^{\delta+}N_2^{\delta-})$ is kinetically stable upon decompression to ambient pressure

after removing helium, making it potentially quenchable to ambient conditions.

This work was supported by the National Science Foundation of China (Grants No. 52025026, No.11874224, No. 52090020, and No. 21803033), the Tianjin Science Foundation for Distinguished Young Scholars (Grant No. 17JCJQJC44400), and the Young Elite Scientists Sponsorship Program by Tianjin (Grant No. TJSQNTJ-2018-18). A.R.O. thanks Russian Ministry of Science and Higher Education (Grant No. 2711.2020.2 to leading scientific schools). X.D. and X.F.Z acknowledge the computing resources of Tianhe II and the support of Chinese National Supercomputer Center in Guangzhou.

[1] M. Miao, Nat. Chem. **9**, 409 (2017).
[2] W. Zhang, A. R. Oganov, A. F. Goncharov, Q. Zhu, S. E. Boulfelfel, A. O. Lyakhov, M. Somayazulu, and V. B. Prakapenka, Science **342**, 1502 (2013).
[3] Q. Zhu, D. Y. Jung, A. R. Oganov, C. W. Glass, C. Gatti, and A. O. Lyakhov, Nat. Chem. **5**, 61 (2013).
[4] M. S. Miao, Nat. Chem. **5**, 846 (2013).
[5] L. Zhu, H. Liu, C. J. Pickard, G. Zou, and Y. Ma, Nat. Chem. **6**, 644 (2014).
[6] X. Dong, A. R. Oganov, A. F. Goncharov, E. Stavrou, S. Lobanov, G. Saleh, G. R. Qian, Q. Zhu, C. Gatti, V. L. Deringer, R. Dronskowski, X. F. Zhou, V. B. Prakapenka, Z. Konôpková, I. A. Popov, A. I. Boldyrev, and H. T. Wang, Nat. Chem. **9**, 440 (2017).
[7] Y. Li, X. Feng, H. Liu, J. Hao, S. A. T. Redfern, W. Lei, D. Liu, and Y. Ma, Nat. Commun. **9**, 722 (2018).
[8] Z. Liu, J. Botana, A. Hermann, S. Valdez, E. Zurek, D. Yan, H. Q. Lin, and M. S. Miao, Nat. Commun. **9**, 951 (2018).
[9] B. Monserrat, M. Martinez-Canales, R. J. Needs, and C. J. Pickard, Phys. Rev. Lett. **121**, 015301 (2018).
[10] J. Lim and C.-S. Yoo, Phys. Rev. Lett. **120**, 165301 (2018).
[11] J. Zhang, J. Lv, H. Li, X. Feng, C. Lu, S. A. T. Redfern, H. Liu, C. Chen, and Y. Ma, Phys. Rev. Lett. **121**, 255703 (2018).
[12] C. Liu, H. Gao, Y. Wang, R. J. Needs, C. J. Pickard, J. Sun, H. T. Wang, and D. Xing, Nat. Phys. **15**, 1065 (2019).
[13] W. L. Vos, L. W. Finger, R. J. Hemley, J. Z. Hu, H. K. Mao, and J. A. Schouten, Nature (London) **358**, 46 (1992).
[14] P. Loubeyre, M. Jean-Louis, R. LeToullec, and L. Charon-Gérard, Phys. Rev. Lett. **70**, 178 (1993).
[15] H. Liu, Y. Yao, and D. D. Klug, Phys. Rev. B **91**, 014102 (2015).
[16] C. Mailhiot, L. H. Yang, and A. K. McMahan, Phys. Rev. B **46**, 14419 (1992).
[17] A. F. Goncharov, E. Gregoryanz, H. K. Mao, Z. Liu, and R. J. Hemley, Phys. Rev. Lett. **85**, 1262 (2000).
[18] W. D. Mattson, D. Sanchez-Portal, S. Chiesa, and R. M. Martin, Phys. Rev. Lett. **93**, 125501 (2004).
[19] M. I. Eremets, A. G. Gavriliuk, I. A. Trojan, D. A. Dzivenko, and R. Boehler, Nat. Mater. **3**, 558 (2004).
[20] M. I. Eremets, A. G. Gavriliuk, and I. A. Trojan, Appl. Phys. Lett. **90**, 171904 (2007).
[21] J. Kotakoski and K. Albe, Phys. Rev. B **77**, 144109 (2008).
[22] C. J. Pickard and R. J. Needs, Phys. Rev. Lett. **102**, 125702 (2009).
[23] Y. Ma, A. R. Oganov, Z. Li, Y. Xie, and J. Kotakoski, Phys. Rev. Lett. **102**, 065501 (2009).
[24] X. Wang, Y. Wang, M. Miao, X. Zhong, J. Lv, T. Cui, J. Li, L. Chen, C. J. Pickard, and Y. Ma, Phys. Rev. Lett. **109**, 175502 (2012).
[25] J. Sun, M. Martinez-Canales, D. D. Klug, C. J. Pickard, and R. J. Needs, Phys. Rev. Lett. **111**, 175502 (2013).
[26] D. Tomasino, M. Kim, J. Smith, and C.-S. Yoo, Phys. Rev. Lett. **113**, 205502 (2014).
[27] B. Hirshberg, R. B. Gerber, and A. I. Krylov, Nat. Chem. **6**, 52 (2014).
[28] A. A. Adeleke, M. J. Greschner, A. Majumdar, B. Wan, H. Liu, Z. Li, H. Gou, and Y. Yao, Phys. Rev. B **96**, 224104 (2017).
[29] D. Laniel, G. Geneste, G. Weck, M. Mezouar, and P. Loubeyre, Phys. Rev. Lett. **122**, 066001 (2019).
[30] D. Laniel, B. Winkler, T. Fedotenko, A. Pakhomova, S. Chariton, V. Milman, V. Prakapenka, L. Dubrovinsky, and N. Dubrovinskaia, Phys. Rev. Lett. **124**, 216001 (2020).
[31] C. Ji, A. A. Adeleke, L. Yang, B. Wan, H. Gou, Y. Yao, B. Li, Y. Meng, J. S. Smith, V. B. Prakapenka, W. Liu, G. Shen, W. L. Mao, and H.-K. Mao, Sci. Adv. **6**, eaba9206 (2020).
[32] H. Olijnyk and A. Jephcoat, J. Phys.: Condens. Matter **9**, 11219 (1997).
[33] S. Ninet, G. Weck, P. Loubeyre, and F. Datchi, Phys. Rev. B **83**, 134107 (2011).
[34] A. R. Oganov and C. W. Glass, J. Chem. Phys. **124**, 244704 (2006).
[35] O. Lyakhov, A. R. Oganov, H. T. Stokes, and Q. Zhu, Comput. Phys. Commun. **184**, 1172 (2013).
[36] See Supplemental Material at http://link.aps.org/supplemental/10.1103/PhysRevB.103.L060102 for an additional electronic property, detailed calculations, and structural parameters.
[37] X.-L. He, X. Dong, Q. S. Wu, Z. Zhao, Q. Zhu, A. R. Oganov, Y. Tian, D. Yu, X.-F. Zhou, and H.-T. Wang, Phys. Rev. B **97**, 100102(R) (2018).
[38] A. R. Oganov, C. J. Pickard, Q. Zhu, and R. J. Needs, Nat. Rev. Mater. **4**, 331 (2019).
[39] J. P. Perdew, K. Burke, and M. Ernzerhof, Phys. Rev. Lett. **77**, 3865 (1996).
[40] G. Kresse and J. Furthmüller, Phys. Rev. B **54**, 11169 (1996).
[41] P. E. Blöchl, Phys. Rev. B **50**, 17953 (1994).
[42] J. Klimeš, D. R. Bowler, and A. Michaelides, Phys. Rev. B **83**, 195131 (2011).
[43] A. Togo and I. Tanaka, Scr. Mater. **108**, 1 (2015).
[44] R. Dronskowski and P. E. Blöchl, J. Phys. Chem. **97**, 8617 (1993).
[45] S. Maintz, V. L. Deringer, A. L. Tchougréeff, and R. Dronskowski, J. Comput. Chem. **37**, 1030 (2016).
[46] X. F. Zhou, G. R. Qian, X. Dong, L. Zhang, Y. Tian, and H. T. Wang, Phys. Rev. B **82**, 134126 (2010).
[47] G. R. Qian, X. Dong, X. F. Zhou, Y. Tian, A. R. Oganov, and H. T. Wang, Comput. Phys. Commun. **184**, 2111 (2013).

[48] W. Tang, E. Sanville, and G. Henkelman, J. Phys.: Condens. Matter **21**, 084204 (2009).
[49] A. R. Oganov, J. H. Chen, C. Gatti, Y. Z. Ma, Y. M. Ma, C. W. Glass, Z. X. Liu, T. Yu, O. O. Kurakevych, and V. L. Solozhenko, Nature (London) **457**, 863 (2009).
[50] K. Nishidate and M. Hasegawa, Phys. Rev. B **86**, 035412 (2012).
[51] M. S. Miao, R. Hoffmann, J. Botana, I. I. Naumov, and R. J. Hemley, Angew. Chem., Int. Ed. **56**, 972 (2016).
[52] S. Yu, B. Huang, Q. Zeng, A. R. Oganov, L. Zhang, and G. Frapper, J. Phys. Chem. C **121**, 11037 (2017).
[53] B. M. Dobratz and P. C. Crawford, *LLNL Explosives Handbook: Properties of Chemical Explosives and Explosive Simulants* (Lawrence Livermore National Laboratory, Livermore, CA, 1985).
[54] M. J. Kamlet and C. Dickinson, J. Phys. Chem. **48**, 43 (1968).
[55] K. Xia, X. Zheng, J. Yuan, C. Liu, H. Gao, Q. Wu, and J. Sun, J. Phys. Chem. C **123**, 10205 (2019).
[56] R. M. Vrcelj, J. N. Sherwood, A. R. Kennedy, H. G. Gallagher, and T. Gelbrich, Cryst. Growth Des. **3**, 1027 (2003).
[57] C. S. Choi and H. P. Boutin, Acta Crystallogr., Sect. B **26**, 1235 (1970).